Science Advances
AAAS

Supplementary Materials for

Observation of quantum superposition of topological defects in a trapped-ion quantum simulator

Zhi-Jie Cheng *et al.*

Corresponding author: Lu-Ming Duan, lmduan@tsinghua.edu.cn

Sci. Adv. **10**, eadr9527 (2024)
DOI: 10.1126/sciadv.adr9527

This PDF file includes:

Supplementary Note: Comparison with a classical random walk model

In Fig. 3 of the main text, we see the interference of the left- and right-going wave packets and the emergence of multiple peaks in the probability distribution of the spin kink. Here we compare it with a classical model to further illustrate their difference. As shown in the main text, in the quantum case for a short evolution time Δt we have a probability amplitude of $-ig\Delta t$ propagating to the neighboring sites. Here for the classical model we similarly assume a probability of $|g|\Delta t$ to hop to each one of the neighboring sites. Also for this classical random walk model we ignore the on-site potential V_n. This simplification is reasonable because we are only interested in the central few sites on which the potential is relatively uniform. Therefore we have the rate equation

$$\frac{d}{dt}p_n(t) = |g| \cdot [p_{n-1}(t) + p_{n+1}(t) - 2p_n(t)] \qquad (n = 2, \cdots, N-2) \tag{S1}$$

and

$$\frac{d}{dt}p_1(t) = |g| \cdot [p_2(t) - p_1(t)], \tag{S2}$$

$$\frac{d}{dt}p_{N-1}(t) = |g| \cdot [p_{N-2}(t) - p_{N-1}(t)]. \tag{S3}$$

Again we start from a spin kink initialized at the center $n = 10$ with $p_n(t = 0) = \delta_{n,10}$. The evolution of the probability distribution at the same time points as Fig. 3 of the main text is shown in Fig. S3. As we can see here, in the classical case we have a diffusive behavior where the wave packet broadens but never splits into multiple peaks. The observation of multiple peaks in the experimental distribution thus verifies the quantum coherence of the superposed spin kinks.

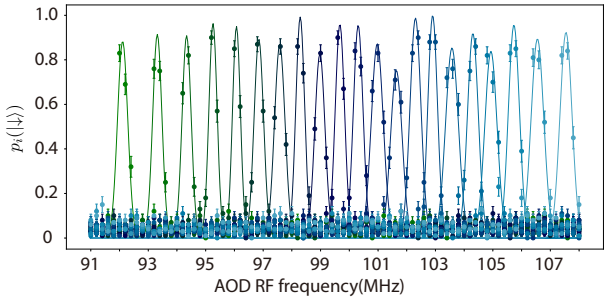

Fig. S1: **Individual addressing of 21 ions using an acousto-optic deflector.** A 370 nm laser pulse embedded in a Ramsey experiment individually addresses a single ion, causing a local AC Stark shift. The i-th ion has a higher probability $p_i(|\downarrow\rangle)$ ending up in $|\downarrow\rangle$ if the individual beam is applied onto this ion. The individual beam location is controlled by the RF frequency of the AOD. By scanning the RF frequency, we calibrate the required frequencies for addressing each ion indicated by the resonances in the plot. Curves in different colors represent the results of different ions.

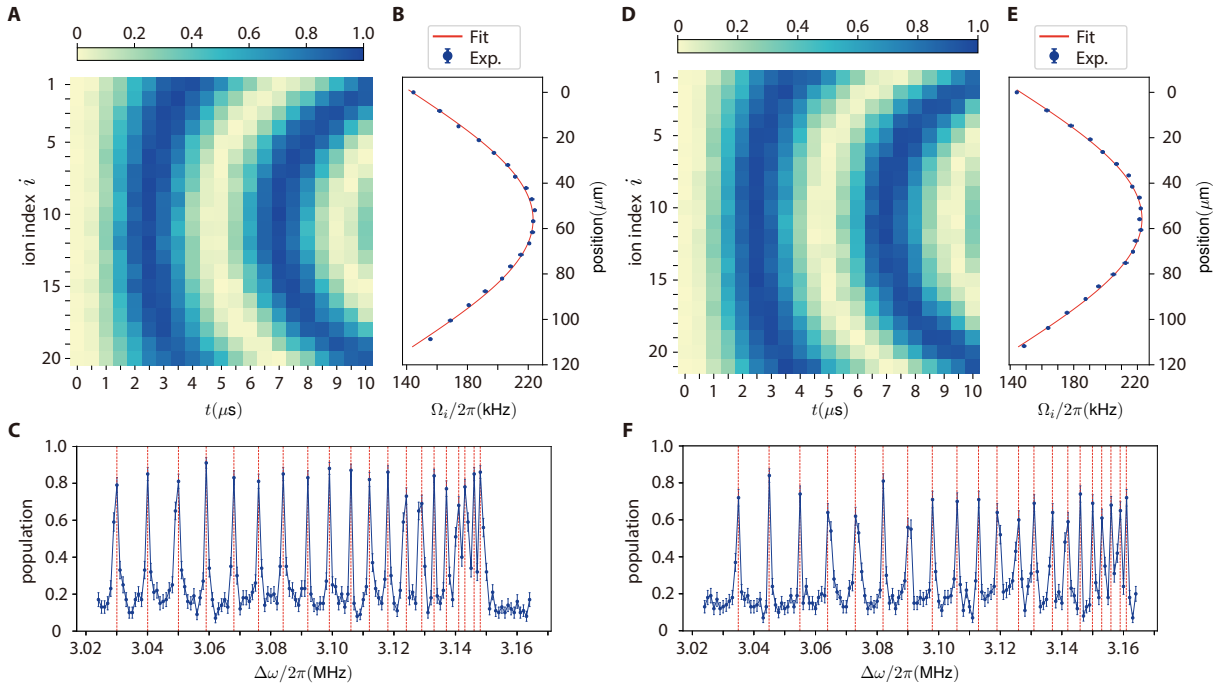

Fig. S2: **Calibration of carrier Rabi frequencies and phonon mode frequencies.** Panels (**A**)-(**C**) and panels (**D**)-(**F**) display the calibration results for a 20-ion chain and a 21-ion chain, respectively. (**A**), (**D**) Heatmaps of carrier transition probabilities for all ions as a function of Raman laser pulse duration. The Rabi oscillations of individual ions are separately fitted to a theory model, yielding their Rabi frequencies, which are shown as blue dots in (**B**) and (**E**). The vertical axis represents ions' position with the origin being the position of the first i on. The measured Rabi frequencies versus the ion position follow a Gaussian distribution whose full width at half maximum is fitted to be around 143 μ m. Fits are shown as red solid l ines. (**C**), (**F**) Blue-sideband spectra (blue dots), which are the transition probability as a function of the detuning $\Delta\omega$ from the carrier transition, are used to extract the phonon mode frequencies (red dashed lines). All data points are with 68% confidence error bars.

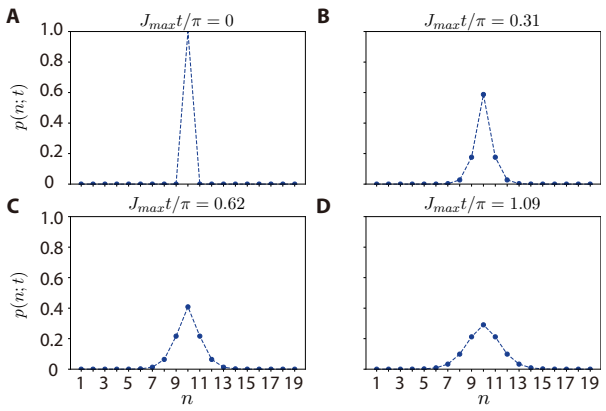

Fig. S3: **Dynamics under a classical random walk model.** (**A**)-(**D**) Population distribution of the kink at different sites $p(n)$ for different evolution times under the same parameters as Fig. 3 of the main text.